Applied Ocean Research 167 (2026) 104944

Contents lists available at ScienceDirect

Applied Ocean Research

journal homepage: www.elsevier.com/locate/apor

Down-scale marine hydrodynamic analysis at the Norwegian coast from metocean to FSI—The NORA-SARAH open framework

Widar Weizhi Wang [a,*], Konstantinos Christakos [b], Csaba Pákozdi [c], Hans Bihs [a]

[a] Norwegian University of Science and Technology, Høgskoleringen 7A, 7491 Trondheim, Norway
[b] Norwegian Meteorological Institute, Allégaten 70, 5007 Bergen, Norway
[c] SINTEF Ocean, Jonsvannsveien 82, 7050 Trondheim, Norway

ARTICLE INFO

Keywords:
Down-scale
Numerical wave modeling
Metocean
Phase-averaging
Phase-resolving
Arbitrary Eulerian–Lagrangian
Hydrodynamic coupling

ABSTRACT

Offshore wave studies often assume Gaussian processes and homogeneous wave fields. However, as waves approach the shoreline, complex coastal topo-bathymetry induces transformations such as shoaling, refraction, diffraction, reflection, and breaking, leading to increased nonlinearity and site-specific wave characteristics. This complexity necessitates detailed site-specific studies for coastal infrastructure design and blue economy planning.

This work presents a dynamical downscaling procedure for analyzing wave–structure interactions from offshore metocean conditions. The open-access NORA3 and NORA10EI hindcast databases define offshore seastates and wind conditions, which are propagated to nearshore regions using the phase-averaged wave model SWAN. The outputs inform phase-resolving simulations with the fully nonlinear potential flow solver REEF3D::FNPF, incorporating an Arbitrary Eulerian–Lagrangian (ALE) method to compute wave forces via Morison's formulation and to screen for severe wave loads, which are further examined using the fully viscous Navier–Stokes solver REEF3D::CFD. A one-way hydrodynamic coupling (HDC) between the potential flow and viscous solvers ensures accurate information transfer.

The proposed NORA-SARAH framework, integrating NORA databases with SWAN-REEF3D-ALE-HDC, offers a robust approach for complex coastal environments. A case study in Southern Norway demonstrates its advantages over traditional significant wave height (H_s)-based or phase-averaged modeling-based practices, highlighting the necessity of this downscaling method.

1. Introduction

The study of offshore wave dynamics has traditionally relied on the assumption of Gaussian processes, treating wave fields as both homogeneous and ergodic. For offshore engineering applications, the characterization of sea states is often conducted using well-established spectral formulations, such as the Pierson–Moskowitz spectrum (Pierson and Moskowitz, 1964) for fully developed seas and the JONSWAP spectrum (Hasselmann et al., 1973) for fetch-limited, developing wave conditions. These spectral models effectively describe deep-water waves; however, as waves propagate towards the coast and interact with complex coastal topo-bathymetry, a series of inter-correlated wave transformations occur, such as shoaling, refraction, diffraction, reflection and breaking. These wave transformations introduce additional nonlinearity and render the wave fields inhomogeneous. Observations from Norwegian coastal waters reveal pronounced inhomogeneities in the wave field, as evidenced by field measurements (Cheng et al., 2021; Christakos et al., 2022) and laboratory experiments (Laflèche et al., 2024). Though corrections can be made on the established spectra to account for the shallow water effects such as the TMA spectrum (Hughes, 1984), it is challenging to formulate a coastal wave spectrum considering the inhomogeneous and nonlinear complex wave fields nearshore. Consequently, coastal wave conditions tend to be highly site-specific, lacking a universally applicable formulation. This limitation poses significant challenges for marine structural design and the planning of blue economy activities, necessitating detailed site-specific investigations to ensure reliable engineering assessments.

One of the first fundamental steps of the site-specific studies is to analyze the meteorology and oceanography (metocean) data at the site of interest. It has been challenging to obtain such data in the past, but increasing efforts at both national and international levels have

* Corresponding author.
E-mail addresses: widar.w.wang@ntnu.no (W.W. Wang), konstantinos.christakos@met.no (K. Christakos), csaba.pakozdi@sintef.no (C. Pákozdi), hans.bihs@ntnu.no (H. Bihs).

https://doi.org/10.1016/j.apor.2026.104944
Received 29 July 2025; Received in revised form 5 November 2025; Accepted 20 January 2026
Available online 2 February 2026

significantly improved data availability through open-access initiatives. In Norway, the Norwegian Meteorological Institute (MET) has played a pivotal role in producing comprehensive metocean datasets that are freely accessible to both industry and the public. Among these datasets, the NORA10 hindcast database provides long-term wind and wave hindcasts for the Norwegian Sea, the North Sea, and the Barents Sea, covering the period from 1957 to 2022 with a spatial resolution of approximately 10 km. This dataset is based on atmospheric downscaling of the ERA-40 reanalysis (Reistad et al., 2011; Aarnes et al., 2012; Furevik and Haakenstad, 2012), and can be accessed through direct requests or via the revised open-access NORA10EI database (Haakenstad et al., 2020). More recently, the NORA3 dataset (Haakenstad et al., 2021; Breivik et al., 2022) has been introduced, offering improved resolution (3 km horizontal spacing), an expanded spatial domain encompassing the Nordic Seas and the Arctic Ocean, and up-to-date wave and wind information. The accessibility of these databases has been further enhanced by the DNORA API (Christakos et al., 2023), enabling seamless integration with open-source wave models such as SWAN (Booij et al., 1999), WAVEWATCH III (Tolman and Chalikov, 1996) and REEF3D (Bihs et al., 2016; Wang et al., 2020a). In addition to regional NORA hindcasts, DNORA also include functions to downscale global reanalysis datasets such as ERA5. Despite these advancements, a significant scale gap persists between metocean databases and the resolution requirements of coastal engineering applications. While metocean datasets provide regional wave characteristics at resolutions between 3 and 10 km, coastal engineering sites themselves can be smaller than 1 km^2. Consequently, crucial hydrodynamic processes that influence wave–structure interactions remain unresolved, as they are typically confined within a single grid cell or data point of the metocean dataset.

To address this scale gap, spectral wave models such as SWAN (Booij et al., 1999) serve as an intermediate tool, translating large-scale metocean conditions into coastal wave characteristics. SWAN's computational efficiency and capability to simulate wind-wave generation, energy dissipation, shoaling, and nonlinear wave-wave interactions make it an essential component of coastal wave modeling. However, despite its strengths, the underlying assumptions in spectral models limit their ability to capture strongly nonlinear wave transformations and pronounced diffraction effects (Holthuijsen et al., 2003). As a result, phase-resolving models become necessary for accurately simulating complex coastal wave fields.

A variety of phase-resolving models have been developed, each with distinct mathematical formulations and assumptions. Many models rely on depth-averaged approaches based on shallow-water equations (SWE), including Boussinesq-type models (Madsen et al., 1991; Madsen and Sørensen, 1992; Nwogu, 1993; Madsen and Schäffer, 1998), non-hydrostatic multi-layer models (Lynett and Liu, 2004; Stelling and Duinmeijer, 2003; Zijlema and Stelling, 2005, 2008; Zijlema et al., 2011), and quadratic non-hydrostatic pressure models (Jeschke et al., 2017; Wang et al., 2020b). However, the shallow-water assumption is not universally applicable, particularly in coastal regions with abrupt bathymetric variations, such as the Norwegian fjords (Wang, 2020). The inherent limitation of SWE-based models is the ability to represent the deep water dispersion relations. In order to achieve better dispersion, Boussinesq models employ higher-order explicit non-hydrostatic pressure terms (Gobbi et al., 2000; Wei et al., 1995). Despite the achievement of modeling waves accurately up to the non-dimensional water depth to wavelength $kd = 40$ presented by Madsen et al. (2002), the multiple expansions lead to a large set of equations and high-order derivatives which limit the numerical stability of the models. The multi-layer models can also achieve much-improved dispersion relation with an increasing number of vertical layers, but often at the cost of significantly increased computational time (Monteban, 2016).

To overcome these limitations, potential-flow-based models, including boundary element methods (BEM) (Grilli et al., 1994, 2001), high-order spectral (HOS) methods (Ducrozet et al., 2012; Bonnefoy et al., 2006a,b; Ducrozet et al., 2016; Raoult et al., 2016; Yates and Benoit, 2015), and fully nonlinear potential flow (FNPF) models (Li and Fleming, 1997; Bingham and Zhang, 2007; Engsig-Karup et al., 2009; Bihs et al., 2020), provide more accurate descriptions of wave dispersion. For large-scale coastal areas with irregular boundaries, the fully populated unsymmetrical matrix in a BEM model is computationally demanding and makes it challenging to implement parallel computation techniques suitable for large domains. In recent developments, the HOS model has improved its ability to represent wave propagation over varying bathymetry and breaking waves (Zhang et al., 2019; Simon et al., 2019) though practical engineering applications are yet to be shown. The finite difference method (FDM)-based FNPF model OceanWaves3D (Engsig-Karup et al., 2009) uses a surface-and-bottom-following σ-grid to represent the varying bathymetry and an adaptive curvilinear grid to represent the irregular coastlines. The model is thus very versatile for coastal applications, especially given the recent GPU acceleration (Engsig-Karup et al., 2012). However, the generation of a curvilinear grid is case-dependent and can be time-consuming. To further the versatility, the REEF3D::FNPF model (Wang et al., 2022a) introduces an innovative level-set-based coastline algorithm that ensures a flexible and efficient representation of coastal boundaries while maintaining a straightforward structured rectilinear horizontal grid. REEF3D::FNPF has also included the steepness-induced and depth-induced breaking wave algorithms to identify breaking waves and represent the breaking wave kinematics and energy dissipation. The efficiency, flexibility, accuracy and stability of the model have been demonstrated for high-order Stokes wave propagation (Wang et al., 2022a), irregular wave simulation (Wang et al., 2021a,b), focused wave generation (Wang et al., 2019) and wave transformations in the coastal waters and harbours (Wang et al., 2022a,a).

Further advancements in numerical modeling have integrated wave–structure interaction (WSI) analysis within phase-resolving frameworks. For instance, the Arbitrary Lagrangian–Eulerian (ALE) method in REEF3D::FNPF enables real-time force estimations on structures without requiring explicit geometric modeling (Pákozdi et al., 2022). This method, utilizing nonlinear wave kinematics and the Morison equation (Morison et al., 1954), facilitates rapid force estimations. With calibrations in mind, the method can be adapted to include slamming loads as well (Pakozdi et al., 2022; Kamath et al., 2023). Though the detailed wave–structure interaction is not resolved, the method can provide force estimation for multiple structures in the efficient wave model REEF3D::FNPF at runtime and presents an opportunity for wind-farm-scale preliminary designs. The irregular wave simulations often require over 3 h of duration for a sufficient statistical representation. Consequently, the ALE approach is able to present 3-hour time series of the wave forces which act as an efficient extreme events identification (EEI) screening. In comparison to traditional H_s-based design procedure, this approach gives time domain information for fatigue calculation, provide spectral information with frequency resonance identification and can resolve short-duration events that have not been represented in the process of H_s calculation.

For extreme limit state designs that require breaking-wave–structure interaction analysis, viscous Navier–Stokes solvers with turbulence models can be employed. These computational fluid dynamics (CFD) models effectively capture complex free surface interactions, including overturning plunging breakers, providing a more comprehensive and detailed slamming load calculation than the calibrated ALE approach. However, these models demand significant computational resources and time. A common strategy to enhance efficiency while maintaining flow detail resolution is coupling a non-viscous solver with a CFD model. For instance, Technip has developed a hydrodynamic coupling (HDC) between its in-house potential flow solver TPNWT and the commercial CFD software StarCCM+ for sea-state statistical analysis (Baquet et al., 2017a). Similarly, the potential flow solver OceanWave3D (Engsig-Karup et al., 2009) has been integrated with the numerical wave tank (NWT) in the CFD solver OpenFOAM (Jacobsen

et al., 2012) to analyze breaking wave forces on a vertical cylinder (Paulsen et al., 2014). The open-source hydrodynamic framework REEF3D offers multiple models and built-in HDC protocols (Wang et al., 2022b), facilitating a more seamless coupling within the same numerical framework while utilizing shared parallelized high-performance computing (HPC) capabilities. The HDC protocol is explained in detail through the example of coupling the fully nonlinear potential flow model REEF3D::FNPF (Wang et al., 2022a) with the CFD solver REEF3D::CFD (Bihs et al., 2016). However, the modular design of the REEF3D framework enables a straightforward extension of the coupling protocol to the non-hydrostatic shallow water equation-based model REEF3D::SFLOW (Wang et al., 2020b) as demonstrated in Dempwolff et al. (2023). The CFD model REEF3D::CFD has undergone extensive validation for various breaking wave interactions with cylindrical and jacket structures (Alagan Chella et al., 2019; Aggarwal et al., 2019, 2020). The HDC procedures effectively link far-field wave kinematics with near-field fluid–structure interaction (FSI) analysis under breaking waves within this framework. However, the previous HDC investigations tend to focus on controlled lab environments with relatively simple bathymetry such as a submerged slope. The HDC method's applicability and practicality in real-world scenarios with natural bathymetry need further demonstrations.

The development of open-access databases, open-source models, and HDC protocols paves the way for a structured approach to downscaling large-scale offshore met-ocean data for near-field FSI analysis of breaking waves. Advancing beyond conventional approaches, this study proposes a streamlined multi-scale synergy that effectively integrates individual models and techniques to establish an efficient connection between metocean data and FSI analysis. The proposed framework is codenamed NORA-SARAH (**NORA**-**S**WAN-**R**EEF3D-**A**LE-**H**DC), which combines the NORA metocean databases, the SWAN phase-averaged wave model, the REEF3D::FNPF phase-resolving wave model, the ALE force estimation method, and the HDC protocol within the REEF3D modeling environment. While each modeling component has been previously investigated, this framework uniquely integrates open-access data and open-source models to facilitate realistic, time-efficient, and adaptable hydrodynamic analyses for coastal and marine structures.

The proposed approach maintains the full nonlinearity of the flow and inherently accounts for breaking wave effects, avoiding reliance on linear wave theory or empirical formulations. A key novelty lies in bridging metocean downscaling and engineering design within a unified framework that connects the offshore sea state directly to local force calculations. Traditionally, these two stages are performed separately by different experts, using a combination of open-source and commercial software, requiring multiple data transfers and format conversions. This fragmented workflow often leads to information loss, interpretation errors, and inconsistencies. In contrast, the present study leverages the synergy of open-source model frameworks to establish an integrated, end-to-end procedure that ensures consistent data exchange and efficient utilization of metocean information throughout the entire modeling chain.

The resulting near-field CFD simulation provides high-resolution insights, demonstrating the feasibility of the HDC protocol in accurately capturing complex wave dynamics over natural bathymetry within a large-scale engineering application. Furthermore, the framework achieves this level of detail while optimizing computational efficiency. A case study in southern Norway demonstrates the workflow and effectiveness of the proposed approach. The findings underscore the necessity of adopting the NORA-SARAH framework, or similar multi-scale methodologies, over conventional spectral wave models or simplified design approaches based on significant wave height (H_s).

2. Numerical models

2.1. Phase-averaging wave model

The SWAN (Simulating Waves Nearshore) model (Booij et al., 1999) is a third-generation spectral wave model designed to simulate wave energy distribution and transformation. It achieves this by solving the spectral action balance equation, which can be expressed in a Cartesian coordinate system as:

$$\frac{\partial}{\partial t}N + \frac{\partial}{\partial x}c_x N + \frac{\partial}{\partial y}c_y N + \frac{\partial}{\partial \sigma}c_\sigma N + \frac{\partial}{\partial \theta}c_\theta N = \frac{S_{tot}}{\sigma}, \tag{1}$$

where N represents the spectral action density, defined as E/σ, with E being the spectral energy density and σ the relative wave frequency in the moving frame of the current. The propagation velocities c_x, c_y, c_σ, and c_θ govern the spatial, frequency, and directional evolution of the spectral action. The term S_{tot} represents the total source term, encompassing the various physical processes influencing wave transformation:

$$S_{tot} = S_{in} + S_{nl3} + S_{nl4} + S_{ds,w} + S_{ds,b} + S_{ds,br}. \tag{2}$$

Here, S_{in} accounts for wind energy input, S_{nl3} and S_{nl4} model triad and quadruplet nonlinear wave-wave interactions, while $S_{ds,w}$, $S_{ds,b}$, and $S_{ds,br}$ represent dissipation mechanisms due to white-capping, bottom friction, and wave breaking in shallow water, respectively.

2.2. Phase-resolving models

The open-source hydrodynamic code REEF3D (Bihs et al., 2016) offers various phase-resolving numerical models, each tailored for different scales and physical phenomena. For large-scale coastal wave propagation, the fully nonlinear potential flow model REEF3D::FNPF (Wang et al., 2022a) is employed, while near-field wave–structure interactions are captured using the computational fluid dynamics (CFD) solver REEF3D::CFD (Bihs et al., 2016).

2.2.1. REEF3D::FNPF

REEF3D::FNPF is based on the solution of the Laplace equation for the velocity potential ϕ:

$$\frac{\partial^2 \phi}{\partial x^2} + \frac{\partial^2 \phi}{\partial y^2} + \frac{\partial^2 \phi}{\partial z^2} = 0. \tag{3}$$

Boundary conditions include kinematic and dynamic free surface conditions and the kinematic bottom boundary condition:

$$\frac{\partial \phi}{\partial z} + \frac{\partial h}{\partial x}\frac{\partial \phi}{\partial x} + \frac{\partial h}{\partial y}\frac{\partial \phi}{\partial y} = 0, \quad z = -h, \tag{4}$$

$$\frac{\partial \eta}{\partial t} = -\frac{\partial \eta}{\partial x}\frac{\partial \widetilde{\phi}}{\partial x} - \frac{\partial \eta}{\partial y}\frac{\partial \widetilde{\phi}}{\partial y} + \widetilde{w}\left(1 + \left(\frac{\partial \eta}{\partial x}\right)^2 + \left(\frac{\partial \eta}{\partial y}\right)^2\right), \tag{5}$$

$$\frac{\partial \widetilde{\phi}}{\partial t} = -\frac{1}{2}\left(\left(\frac{\partial \widetilde{\phi}}{\partial x}\right)^2 + \left(\frac{\partial \widetilde{\phi}}{\partial y}\right)^2\right) + \frac{1}{2}\widetilde{w}^2\left(1 + \left(\frac{\partial \eta}{\partial x}\right)^2 + \left(\frac{\partial \eta}{\partial y}\right)^2\right) - g\eta, \tag{6}$$

where the velocity potential and the vertical velocity at the free surface η are identified with a tilde $\widetilde{\phi}$ and $\widetilde{w}$ and the horizontal coordinate is written as $\mathbf{x} = (x, y)$.

The model employs a finite difference approach and utilizes the BiCGStab solver (van der Vorst, 1992) preconditioned with the geometric multigrid solver PFMG (Ashby and Flagout, 1996) from the hypre library. While the horizontal grid remains rectilinear, a σ-grid is implemented in the vertical direction, ensuring increased resolution near the free surface:

$$\sigma = \frac{z + h(\mathbf{x})}{\eta(\mathbf{x}, t) + h(\mathbf{x})}, \tag{7}$$

where $h(\mathbf{x})$ is the local wave depth in the Cartesian coordinate.

Wave breaking is identified using depth- and steepness-based criteria (Zijlema et al., 2011; Smit et al., 2013), and energy dissipation is introduced through an artificial viscous term (Baquet et al., 2017b).

Coastlines are captured using a level-set function, allowing a smooth transition between wet and dry cells, which are designated with opposite signs and identified based on a local water depth threshold.

2.2.2. Arbitrary Eulerian-Lagrangian (ALE) force calculation

The σ-grid formulation provides precise free surface locations, enabling the representation of nonlinear wave kinematics in an Arbitrary Eulerian–Lagrangian (ALE) framework (Donea et al., 2004; Pákozdi et al., 2022). Following the ALE approach, the fluid particle acceleration is written as:

$$a_x = \left.\frac{\partial u}{\partial t}\right|_{\vec{\sigma}} + u\left(\frac{\partial u}{\partial \xi} + \frac{\partial u}{\partial \sigma}\frac{\partial \sigma}{\partial x}\right) + \left(w - \sigma\left.\frac{\partial \eta(x,t)}{\partial t}\right|_{\vec{x}}\right)\frac{\partial u}{\partial \sigma}\frac{\partial \sigma}{\partial z}, \tag{8}$$

where the horizontal and vertical velocities and coordinates are u, w, ξ and σ respectively.

The nonlinear wave velocity and accelerations absence from the disturbance from the structures integrated the Morison equation for rapid wave forces calculations:

$$F_x = \rho(h+\eta)\left[\int_0^1 C_M a_x A_{xy} d\sigma + \int_0^1 C_D u|u|\frac{1}{2}B_p d\sigma\right], \tag{9}$$

where C_M and C_D are inertia and drag coefficients, while A_{xy} and B_p denote the cross-section area and section width.

With calibrations, the adapted form of the ALE method can even account for slamming loads as well (Pakozdi et al., 2022; Kamath et al., 2023).

2.2.3. REEF3D::CFD

REEF3D::CFD (Bihs et al., 2016) employs a finite difference method to solve the Navier–Stokes equations:

$$\frac{\partial u_i}{\partial x_i} = 0, \tag{10}$$

$$\frac{\partial u_i}{\partial t} + u_j\frac{\partial u_i}{\partial x_j} = -\frac{1}{\rho}\frac{\partial p}{\partial x_i} + \frac{\partial}{\partial x_j}\left[(\nu+\nu_t)\left(\frac{\partial u_i}{\partial x_j} + \frac{\partial u_j}{\partial x_i}\right)\right] + g_i, \tag{11}$$

where u represents the velocity of the fluid particles, ρ is the fluid density, p is pressure, ν denotes the kinematic viscosity, ν_t is the eddy viscosity, and g accounts for gravitational acceleration.

The pressure solution is obtained using Chorin's projection method (Chorin, 1968), and the Poisson equation is handled via the BiCGStab solver (van der Vorst, 1992), preconditioned with the geometric multigrid PFMG from the hypre library for enhanced computational efficiency.

This two-phase model resolves both water and air domains. The free surface, representing the interface between these two phases, is captured through the level-set function (Osher and Sethian, 1988), which is defined as a signed distance function:

$$\phi_l(\vec{x},t)\begin{cases} > 0 \; if \; \vec{x} \in phase \; 1, \\ 0 \; if \; \vec{x} \in \Gamma, \\ < 0 \; if \; \vec{x} \in phase \; 2. \end{cases} \tag{12}$$

The distance function property is maintained by ensuring the validity of the Eikonal equation $|\nabla\phi_l| = 1$.

REEF3D::CFD incorporates a range of turbulence models, including Reynolds-averaged Navier–Stokes (RANS), large-eddy simulations (LES), and direct numerical simulations (DNS). For the present study on breaking wave interactions, the RANS approach with the two-equation k-ω model (Wilcox, 1994) is applied.

Both REEF3D models implement high-order numerical schemes for improved accuracy. The fifth-order WENO (weighted essentially non-oscillatory) scheme (Jiang and Shu, 1996) is used for spatial discretization, while the third-order Runge–Kutta scheme (Shu and Osher, 1988) is adopted for temporal advancement. These high-order schemes are particularly beneficial for accurately capturing steep and nonlinear wave characteristics.

The two phase-resolving models also share wave generation methods. Surface waves can be generated following the relaxation zone method (Larsen and Dancy, 1983; Mayer et al., 1998) where one characteristic wavelength is typically used as the relaxation zone length (Bihs et al., 2016). To reduce the cell counts, boundary conditions prescribing wave kinematics and surface elevations can be used for wave generation as well, specifically a Dirichlet boundary condition for the CFD model and a Neumann boundary condition for the FNPF model. To mitigate undesired reflections from the outlet boundaries, a relaxation zone is often used as a numerical beach following a reverse process of the wave generation relaxation zone. Alternatively, active absorptions can be utilized to cancel the incident waves following the shallow water linear wave theory.

Furthermore, all REEF3D models are fully parallelized using domain decomposition, with subdomains communicating through the Message Passing Interface (MPI) protocol. This enables highly scalable simulations, allowing for efficient utilization of large numbers of processors to significantly enhance computational speed.

2.2.4. Hydrodynamic Coupling (HDC)

Within the REEF3D framework, a one-way coupling strategy facilitates the transfer of simulation data between different models (Wang et al., 2021c; Dempwolff et al., 2023). During the FNPF simulation, the hydrodynamic state at each time step or iteration is stored in dedicated state files covering the entire computational domain. The velocity components derived from the velocity potential together with the surface elevation are stored in the state files, which are linearly interpolated from the σ-coordinate grid in the non-viscous domain to the Cartesian grid used in the viscous CFD numerical wave tank (NWT). The interface boundary between the domains can be performed either following a relaxation zone strategy or by a Dirichlet boundary. The CFD simulation can then be performed using the stored flow data, employing either the same number of processors as the FNPF run or an entirely different high-performance computing (HPC) configuration. The workflow schematic of the HDC procedure is summarized in Fig. 1.

This approach enhances computational flexibility, allowing multiple CFD simulations to be initiated from different time points and spatial locations while leveraging data from a single FNPF simulation. As a result, overall computational efficiency is improved by maximizing data reusability and minimizing redundant simulations. The synergy between these models ensures a streamlined workflow for detailed hydrodynamic analysis of breaking wave interactions.

3. The NORA-SARAH framework

The open-access met-ocean databases NORA10EI and NORA3 serve as essential sources of offshore environmental data, which can be systematically downscaled for near-field wave–structure interaction analysis. This information propagation is facilitated by a sequence of open-source numerical models. The open-source metocean-api (https://github.com/MET-OM/metocean-api) provided by MET is used to extract met-ocean conditions from the NORA3 wind and wave database for a specified location and time window, converting them into compatible inputs for wave models such as SWAN and REEF3D. This process is automated using the open-source tool DNORA, which can download and prepare boundary conditions (wind, wave, surface current, and ice) for multiple locations and extract bathymetry based on specified coordinates. The phase-averaging model SWAN provides statistical wave characteristics and bridges offshore and nearshore wave conditions. In contrast, the phase-resolving REEF3D::FNPF model captures nonlinear wave transformations influenced by seabed variations and coastal features. For wave load assessment, the ALE method operates in real-time within REEF3D::FNPF simulations, estimating wave-induced forces for preliminary design and extreme event identification (EEI). The wave kinematics computed within the FNPF numerical wave tank (NWT) are then mapped onto the computational domain of the viscous CFD solver REEF3D::CFD, enabling detailed analysis of breaking-wave-induced forces under extreme conditions. This integrated workflow, referred to as the NORA-SARAH approach (**NORA**-**S**WAN-**R**EEF3D-**A**LE-**H**DC),

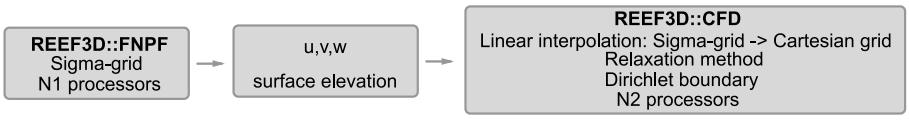

Fig. 1. A schematic representation of the HDC procedure between the non-viscous and viscous solvers.

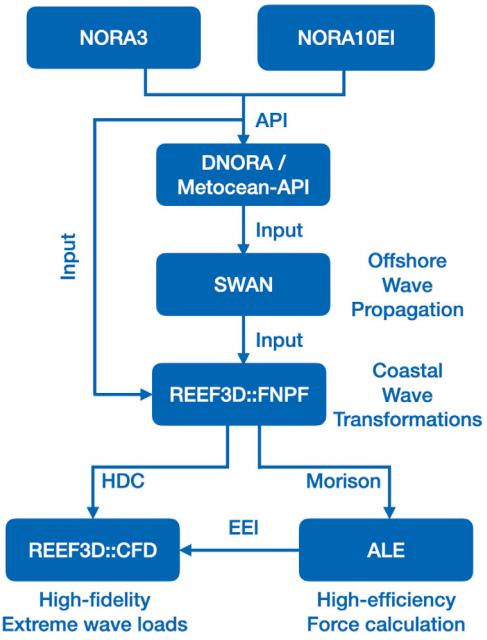

Fig. 2. Schematic representation of the NORA-SARAH framework (NORA-SWAN-REEF3D-ALE-HDC), illustrating the integration of offshore hindcast data with numerical modeling for marine structure wave load estimation.

structures the transition from large-scale offshore hindcast data to high-fidelity numerical modeling for wave load estimation, as illustrated in Fig. 2.

The subsequent section demonstrates the effectiveness of this framework through a case study on the southern Norwegian coast.

4. Hydrodynamic analysis in southern Norway

The selected study site for demonstrating the NORA-SARAH framework is the water body surrounding the island of Store Lyngholmen, located near Kristiansand in southern Norway. The location, along with its surrounding topographic and bathymetric environment, is illustrated in Fig. 3. Situated at Norway's southern tip, the site is exposed to southern swell and wind waves originating from both the Atlantic Ocean to the west and the Skagerrak Strait to the east, which serves as a connection between the Atlantic Ocean and the Baltic Sea.

A navigation tower, marked as a red triangle in Fig. 3, is proposed to be constructed on a shoal known as Lyngholmsboen (58.052004°N, 7.925912°E), located southeast of Store Lyngholmen. This shoal features a peak water depth of approximately 5 m, while the surrounding waters reach depths of roughly 50 m. Constructing the tower in this shallow-water region offers advantages such as reduced material requirements and lower construction costs. However, the presence of the shoal also influences wave behavior, leading to wave shoaling, refraction, and an increase in wave energy concentration. These effects can introduce nonlinear wave kinematics and higher-order wave harmonics. The horizontal distance from the shoal's peak to the 50 m depth contour to the south is approximately 185 m, resulting in a submarine slope of about 1:4. This relatively steep slope poses challenges related to wave breaking and potential slamming loads on the structure. The NORA-SARAH framework will be employed to analyze wave conditions and wave-induced loads, including slamming effects on the tower.

On the leeward side of Store Lyngholmen, an anchorage site (58.0579741°N, 7.920036°E) is marked as a red circle in Fig. 3. The satellite image in the center-lower panel of Fig. 3 shows reduced wave activity in the diffraction zone on the northern side of the island. However, varying wave conditions can result in different diffraction intensities and changes in wave energy distribution across frequencies due to the non-uniform nature of the diffracted wave field. As discussed in the introduction, traditional spectral wave models often fail to capture diffraction effects in sufficient detail. Consequently, wave conditions at the anchorage site will also be analyzed using the NORA-SARAH framework.

The downscaling analysis following the NORA-SARAH strategy is summarized and visualized in Fig. 4. Metocean data is obtained from an offshore location (58.00711°N, 7.93309°E), marked as a yellow star in the left panel of Fig. 4, using metocean-api linked to the NORA3 wind and wave hindcast database. This location is situated near the 100 m depth contour, representing intermediate to deep water conditions for most offshore irregular wave components. The site is approximately 4 km from the Lyngholmsboen shoal, exceeding the 3 km resolution of NORA3, ensuring adequate metocean data interpolation. The local significant wave height and peak period information between 2024-01-01 and 2024-06-30 are obtained and summarized in Fig. 5. For the purpose of demonstration, long-crested waves coming from 180° south are assumed during the period despite the actual temporal variations. It is seen that the most severe sea state is observed in the winter season, especially during late January, where a maximum significant wave height (H_s) and peak period (T_p) combination is recorded as highlighted in the blue box in Fig. 5. The maximum H_s and T_p are 6.88 m and 13.67 s, which are used as input parameters for the offshore phase-averaged SWAN simulations.

The SWAN simulation domain, outlined as a blue box in Fig. 4, extends 7 km northward from the wave input location at its southern boundary, with an east–west span of 4.5 km. This domain encompasses key topo-bathymetric features that significantly influence wave propagation and transformation toward the site of interest. To ensure uniform offshore wave generation and minimize diffraction effects near the generation boundary, wave input is applied at three boundaries: south, west, and east. To ensure a representative offshore condition and minimize diffraction effects near the generation boundary, the maximum H_s and T_p at the west and east side boundaries under the same time incidence are applied at the side boundaries: H_s = 5.78 m and T_p = 13.52 s at coordinate (434 000, 6.433E6) and H_s = 6.08 m and T_p = 13.59 s at coordinate (438 500, 6.433E6). The imposed long-crested wave field at 180° is approximated in SWAN by setting the power parameter m to 130 in the $cos^m(\theta - \theta_{peak})$ directional spreading function, corresponding to a 5° standard deviation in directional spreading.

A horizontal resolution of 10 m is used in the SWAN simulations. The directional sector from 90° to 270° is discretized into 72 bins, each with an angular resolution of 2.5°. The frequency range spans from half the peak frequency to three times the peak frequency, resulting in a range of [0.035, 0.215] Hz, discretized with 0.001 Hz intervals. The wave spectrum follows a JONSWAP distribution, an appropriate assumption given the site's exposure to the North Atlantic Ocean. The simulation is conducted as a stationary case without additional wind forcing.

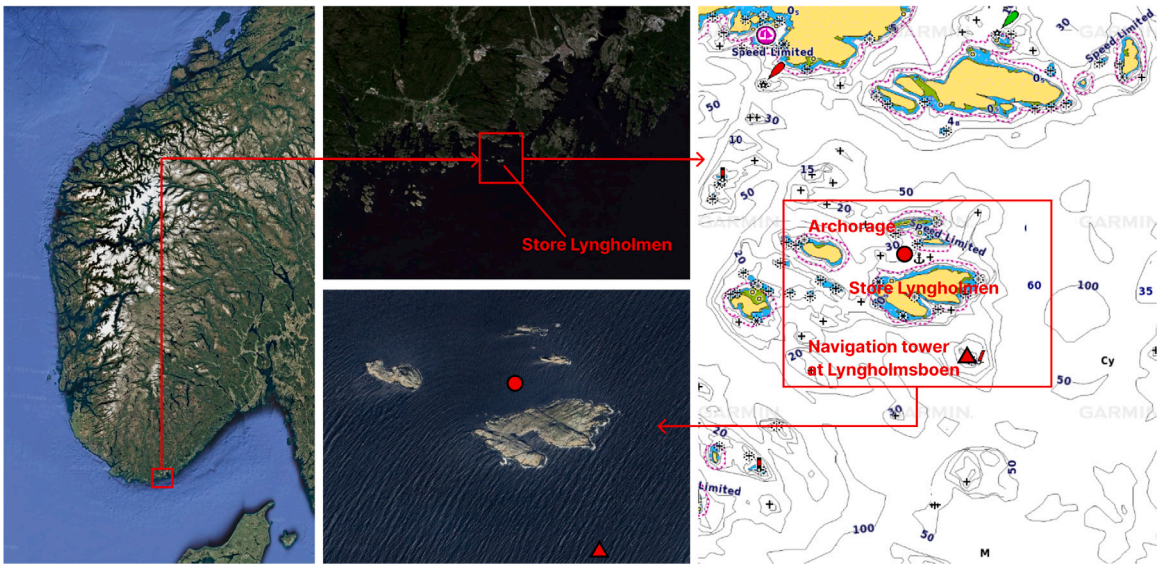

Fig. 3. Study site near the island of Store Lyngholmen in southern Norway. The left and center-upper panels display satellite images of the island and its surroundings, sourced from the Norwegian Mapping Authority (www.norgeskart.no). The right panel provides bathymetric data of the adjacent area, obtained from the Garmin Sea Chart (https://maps.garmin.com/nb-NO/marine). The center-lower panel presents a satellite snapshot from Google Earth (https://earth.google.com/web), capturing wave propagation and diffraction around the island. The navigation tower location is marked with a red triangle, and the anchorage site is indicated with a red circle.

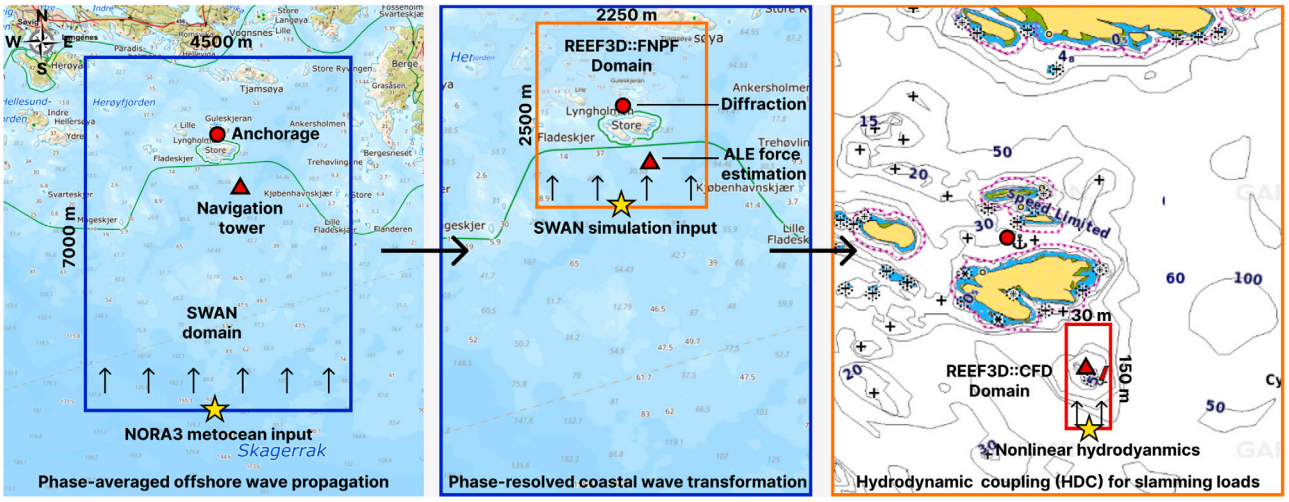

Fig. 4. The down-scale process with reduced domain sizes from the phase-averaged offshore wave propagation simulation with SWAN (marked as a blue box) to the phase-resolved coastal wave transformation simulation with REEF3D::FNPF (marked as an orange box) further to the near-field fluid–structure interaction simulation using REEF3D::CFD (marked as a red box) follow an HDC protocol with Dirichlet coupling boundary conditions. The yellow stars represent the wave input between the scales.

The spatial distribution of significant wave height (H_s) within the simulation domain is illustrated in Fig. 6. While the offshore wave field remains homogeneous, bathymetry-induced wave transformations become evident in shallower waters. Notable increases in H_s occur at multiple shoals are observed, including Lyngholmsboen, where the navigation tower is located. The SWAN output at the phase-resolving boundary, indicated by the yellow star in the center panel of Fig. 4, is used to define the input wave conditions for the REEF3D::FNPF numerical wave tank (NWT), represented by the orange box in Fig. 4.

The phase-resolving REEF3D::FNPF numerical wave tank (NWT) has a domain size of 2500 × 2250 m, which is less than one-quarter of the SWAN simulation domain. It focuses on the region surrounding Store Lyngholmen to provide detailed insights into wave transformations and estimate wave loads. The numerical representation of the local bathymetry and the NWT configuration are illustrated in Fig. 9. The solid-line black box denotes the 400 m relaxation zone for wave generation, designed to accommodate two wavelengths corresponding to the peak period. The dashed-line black boxes indicate relaxation zones acting as numerical beaches to dissipate wave energy at the three remaining boundaries. The side boundaries feature 200 m relaxation zones, while the northern boundary along the principal wave propagation direction has a relaxation zone of 400 m.

Three wave gauges are deployed within the NWT, as shown in Fig. 9(d). The red cube represents the wave gauge used to verify the input waves, the triangle indicates the wave gauge located at the navigation tower's center, and the circle marks the wave gauge positioned at the anchorage site. The domain is discretized with a uniform horizontal cell size of 5 m and 10 vertical cells, applying a stretching factor of 2.5 to refine resolution toward the free surface, resulting in a total of 2.25 million computational cells. Adaptive time stepping is implemented

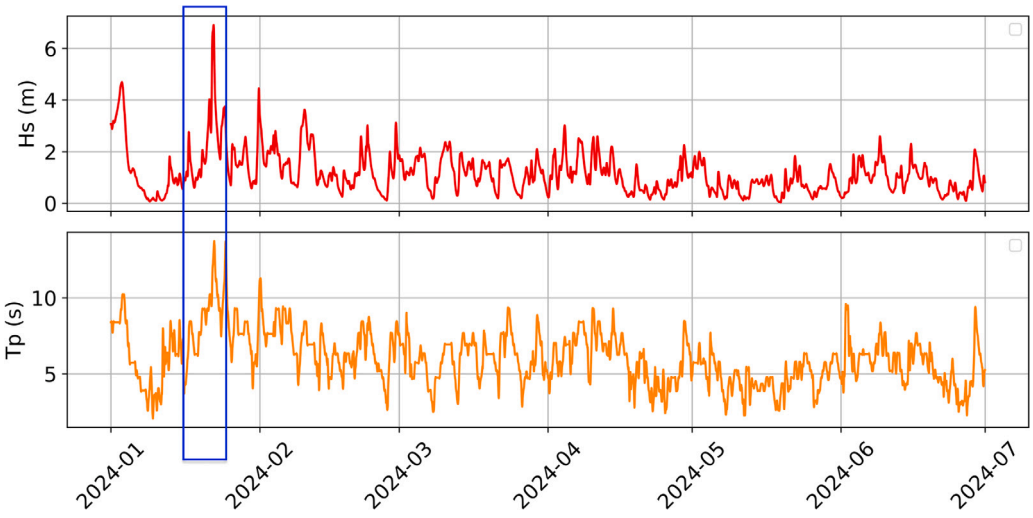

Fig. 5. The offshore H_s and T_p time series between 2024-01-01 and 2024-06-30.

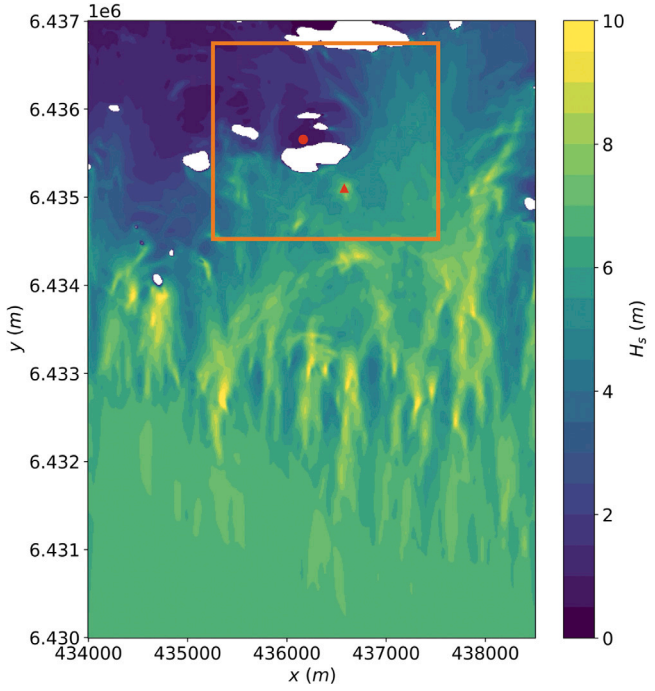

Fig. 6. H_s distribution from the SWAN simulation with the NORA3 inputs. The orange box shows the REEF3D phase-resolving simulation domain within the SWAN domain.

with a Courant–Friedrichs–Lewy (CFL) number of 1.0 to control time step sizes. The grid and CFL convergence of H_s at the navigational tower are presented in Fig. 7. The results indicate that a cell size of 5 m yields a converged solution, and the CFL number has a negligible effect in this case.

The input wave conditions are derived from the SWAN output and parameterized as a JONSWAP spectrum with H_s = 6.0 m and T_p = 12.0 s. The frequency range of [0.04, 0.25] Hz is discretized with 1024 frequency components. The simulation runs for 3.6 h (12 800 s), with the last 3 h (10 800 s) of free surface elevation data used for post-processing and wave spectrum reconstruction via Fast Fourier Transform (FFT). The computations are executed using 128 AMD EPYC 7763 cores on an Ubuntu-based workstation, achieving an elapsed runtime of 4.5 h.

To compare model representations of coastal wave transformations, a reference SWAN simulation is also performed using the same wave input, domain size, and horizontal grid resolution. Neither simulations are performed with particular calibration, and both have ignored the effects of the bottom friction. The H_s distribution from the SWAN simulation and the final free surface elevation at 12 800 s from the REEF3D::FNPF simulation are shown in Fig. 9. Both models capture the shoaling effects at Lyngholmsboen, but the diffraction patterns on the leeward side of Store Lyngholmen differ significantly. The reference SWAN simulation exhibits a more discrete energy distribution in the diffraction zone, whereas the phase-resolving approach in REEF3D::FNPF presents a more continuous redistribution of wave energy. The choice of the cell size in the SWAN simulation is further supported in a grid convergence study shown in Fig. 8. However, it is worth noting that calibration based on specific scenarios may yield different results and lead to varying comparisons. Since each coastal region has unique conditions, the relative differences presented here should not be interpreted as universally applicable.

The wave spectra recorded at the three wave gauges in REEF3D::FNPF are compared to the input wave spectrum in Fig. 10. The first wave gauge closely matches the input wave spectrum across all frequencies, with fluctuations reflecting the influence of varying bathymetry within the wave generation zone. At the navigation tower gauge, a pronounced energy increase near the peak frequency confirms shoaling effects. Conversely, the spectrum at the anchorage exhibits significantly reduced energy due to diffraction. However, discrepancies arise in the diffraction zone between phase-averaging and phase-resolving approaches.

A comparison of H_s and spectra at the anchorage between the two modeling approaches is presented in Fig. 11. Despite incorporating triad wave–wave interactions, the phase-averaged approach significantly underestimates H_s, whereas the phase-resolving method captures a three-peaked spectrum, revealing interactions between wave systems in the island's lee and nonlinear energy redistribution. This three-peak pattern is crucial for structural design and moored vessel safety, as it highlights potential resonance frequencies that could induce large motions. In contrast, the phase-averaging approach suggests only minor spectral modifications, resembling the input single-peak JONSWAP spectrum with reduced magnitude. For engineering applications, the phase-resolving model provides a more conservative wave condition estimate and identifies dominant wave frequencies, aiding in the design of structures to avoid resonance-related risks.

In addition to the downscaling approach, the larger SWAN simulation domain (blue box in Fig. 4) is also simulated using the phase-resolving potential flow solver, providing a fully phase-resolved reference solution. The free surface elevation at the last time step is shown

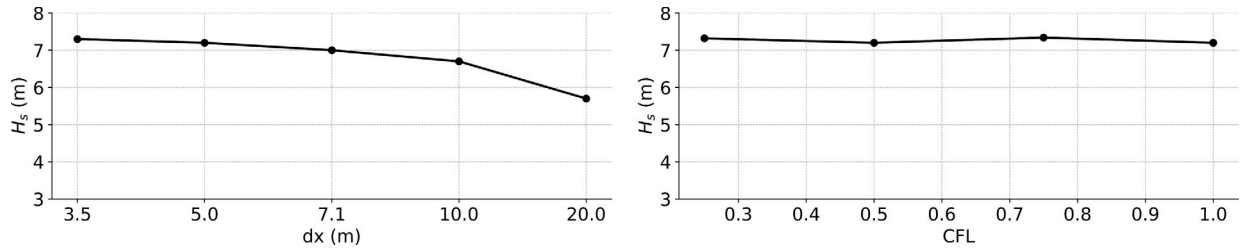

(a) grid convergence (b) CFL convergence

Fig. 7. Grid and CFL convergence for REEF3D::FNPF simulations at the navigational tower.

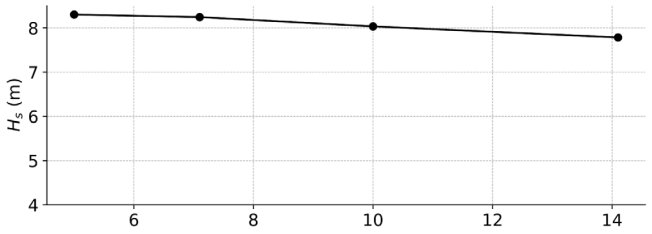

Fig. 8. Grid convergence study for the SWAN simulation at the navigational tower.

in Fig. 12. The shallow offshore shoals induce strong disturbances to the incident waves due to the combined effects of shoaling and refraction, resulting in an inhomogeneous wave field seaward of the downscaling interface. The simulated H_s is compared to the down-scale appraoch at the verification gauge, navigational tower and anchorage, as shown in Fig. 13. The two approaches exhibit similar results at the three gauges, with the largest discrepancy of approximately 10% occurring in the shoaling region.

The conceptual navigation tower has a radius of 3 m, with an inertia coefficient of $C_M = 1.5$ and a drag coefficient of $C_D = 0.9$. The structure itself is not explicitly resolved within the FNPF NWT. Instead, the Arbitrary Lagrangian–Eulerian (ALE) force estimation method is used to compute wave loads in real time, utilizing undisturbed, fully nonlinear wave kinematics from the potential flow solver. The resulting total force time series is depicted in Fig. 14. Unlike the free surface elevation time series, the total force time series directly reflects extreme load events by accounting for wave kinematics in addition to surface elevation effects. In a traditional approach, the SWAN simulated H_s and T_p are used as input parameters to reconstruct an irregular wave field based on the linear wave theory and apply the Morison equation for force calculation based on the reconstructed irregular wave time series. The x-direction inline force derived from the traditional approach is compared with the proposed approach, as shown in Fig. 15. It is seen that the traditional force calculation shows a strong symmetry due to the linear nature and fails to capture the nonlinear peaks.

The spectra of the x- and y-components of the total force are shown in Fig. 16. The force along the x-axis is significantly larger than that in the y-direction. Both spectra reveal a secondary peak at a higher frequency than the peak wave frequency, indicating the potential presence of high-frequency ringing. A time window from 8900 s to 9000 s, highlighted in Fig. 14, shows particularly large wave forces, likely due to wave breaking and slamming on the structure. To investigate this phenomenon in greater detail, this period is analyzed using the fully viscous CFD solver REEF3D::CFD.

To optimize computational efficiency, a near-field domain is selected for the CFD simulation, represented by the red box in the right panel of Fig. 4. This localized approach significantly reduces the coupling data output from REEF3D::FNPF and improves the efficiency of grid interpolation between the FNPF and CFD domains. A Dirichlet boundary condition is applied to transfer wave kinematics and surface elevation data between the solvers in a one-way coupling approach. The mesh configurations in both domains are shown in Fig. 17.

The CFD simulation with REEF3D::CFD is conducted within a 150 × 30 m domain, discretized using a uniform cell size of 0.5 m, resulting in approximately 20.52 million computational cells. In this simulation, the navigation tower is fully resolved. A wave gauge is placed 6 m upstream from the tower center to capture the wave conditions. To estimate wave loads, a 6 × 6 m force box is centered around the tower, integrating pressure fields over the wetted surface.

The CFD simulation initializes flow conditions at 8900 s based on interpolated data from the FNPF domain and runs for 100 s. Due to the complexity of breaking waves, a strict CFL criterion of 0.1 is applied. The simulation is executed on the Betzy supercomputer, using 512 AMD EPYC 7742 cores (2.25 GHz) running on a Red Hat system, with a total computation time of 7.8 h.

The free surface elevation and wave forces computed through the HDC protocol in the CFD simulation are compared with the FNPF results in Fig. 18. Two significant force events are identified in Fig. 18(b). The latter corresponds to a large wave crest, while the first extreme event occurs despite moderate wave crest heights in both the FNPF and CFD simulations. To investigate further, these extreme load events are visualized using ParaView at $t = 8958.1$ s and $t = 8985.0$ s, as shown in Fig. 19. In both cases, plunging breaking waves impact the structure with high velocities, confirming slamming wave loads.

A comparison of surface elevation profiles at these time points is presented in Fig. 20. The first event ($t = 8958.1$ s) exhibits a relatively lower wave crest height, consistent with free surface elevation observations. Similarly, maximum run-up levels are compared, showing that the second event at $t = 8985.0$ s results in greater wetted surface area and larger run-up. However, the velocity magnitude during the first event reaches 15.85 m/s—approximately 30% higher than the second event, where the maximum velocity is 12.22 m/s. This higher velocity magnitude is likely responsible for the increased wave force observed in the first event.

This analysis highlights that extreme wave forces, particularly slamming loads, are not solely correlated with wave crest height or surface elevation. Instead, wave breaking dynamics, shape, and velocity magnitude play crucial roles. The HDC protocol and CFD simulation provide the necessary flow details to accurately capture and explain these hydrodynamic phenomena, offering valuable insights for structural design and wave impact assessments.

The time efficiency of the entire NORA-SARAH down-scale wave modeling approach is summarized in Table 1. The approach combines the strengths of different model types, switching scales with the consideration of the level of resolved physical details and computational efficiency. As a result, the entire process can be performed within 13 h. In comparison, the fully phase-resolving simulation of the entire offshore domain (Fig. 12) requires 512 AMD EPYC 7742 cores (2.25 GHz) and an elapsed time of 11.4 h. If the CFD simulation is extended to the full SWAN domain, it would involve approximately 138 billion computational cells with the current resolution, which is impractical with existing computational resources.

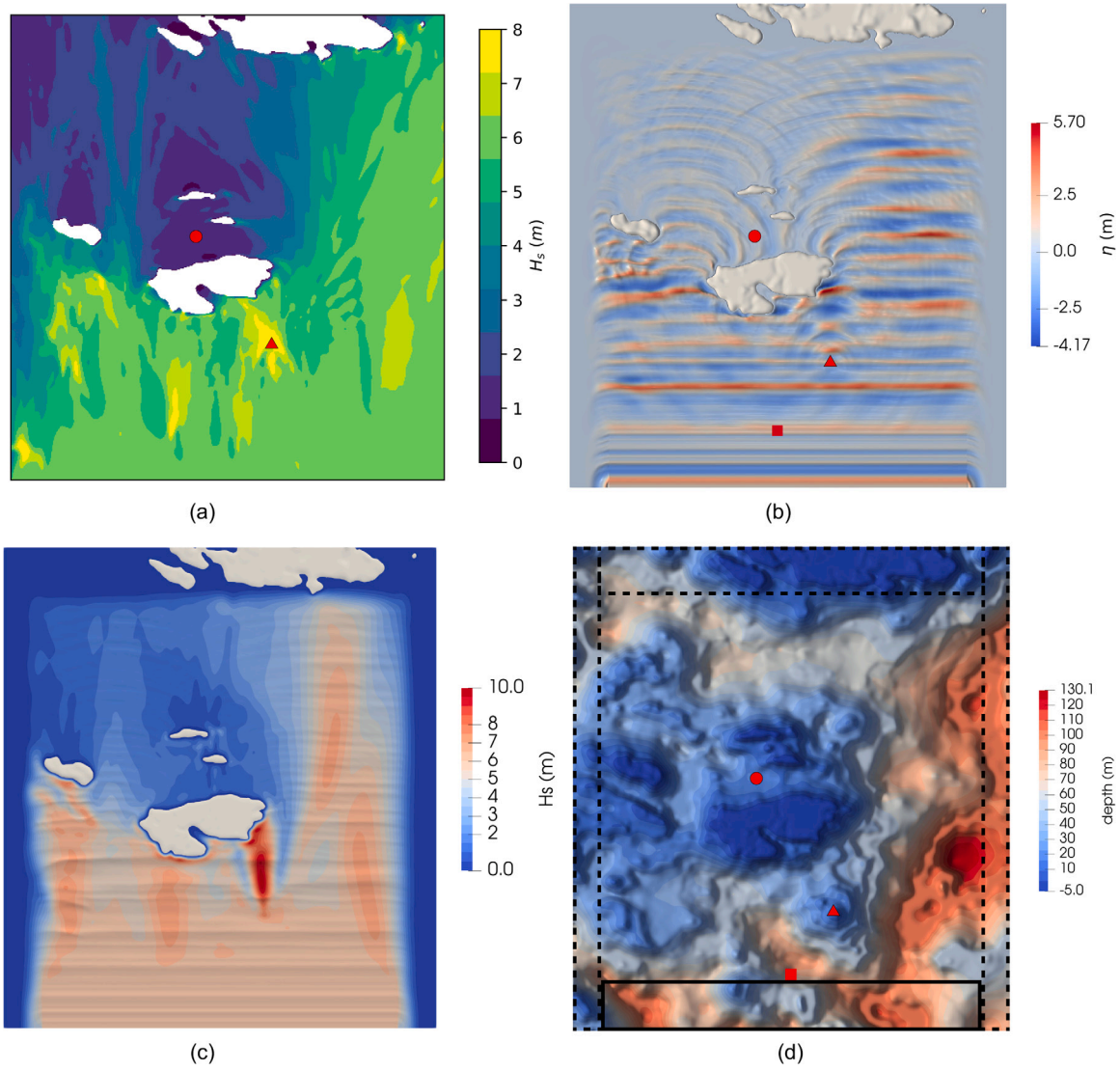

Fig. 9. (a) The H_s distribution from the phase-averaging SWAN simulation, (b) free surface elevation at 12 800 s from the phase-resolving REEF3D::FNPF simulation, (c) The H_s distribution from the phase-resolving REEF3D::FNPF simulation, (d) the configuration and bathymetry of the potential flow solver domain.

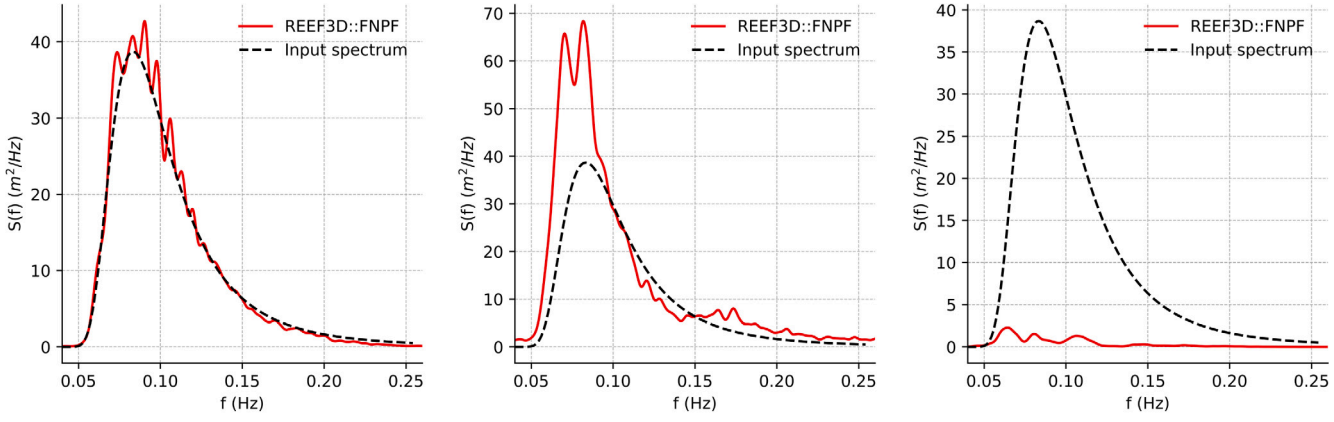

(a) Verification wave gauge □ (b) Navigation tower wave gauge △ (c) Anchorage wave gauge ○

Fig. 10. The wave spectra obtained from the FFT analysis for the free surface elevation time record in the phase-resolving simulation with REEF3D::FNPF.

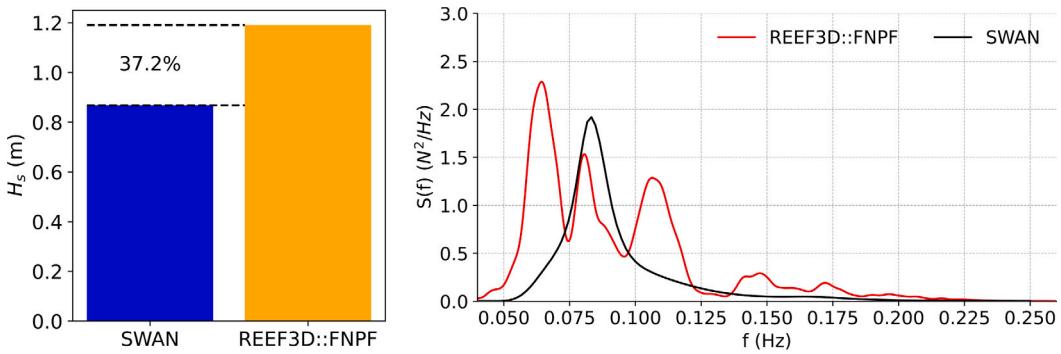

(a) H_s (b) Wave spectra

Fig. 11. The comparison of the H_s and wave spectra at the anchorage from the phase-averaging and phase-resolving approach.

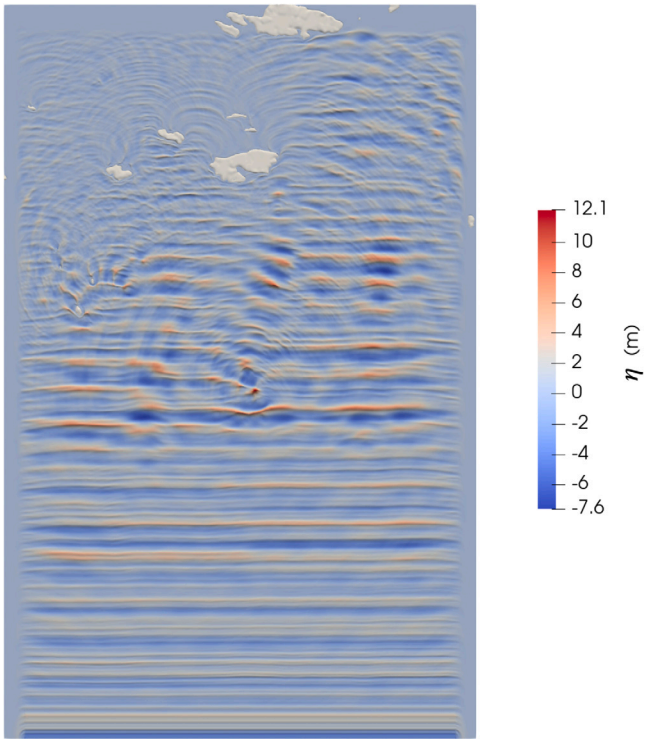

Fig. 12. The free surface elevation at the last time step of the potential flow simulation in the offshore domain to provide a fully phase-resolving solution as a reference to the downscale approach.

Table 1
Simulation time and elapsed time during the NORA-SARAH down-scale wave modeling procedure.

	SWAN (offshore)	REEF3D::FNPF	REEF3D::CFD
Simulation time	Stationary	3.6 h	100 s
Elapsed time	0.7 h	4.5 h	7.8 h
Computational resource	4 × M4 Max	128 × AMD	512 × AMD

5. Conclusion

The NORA-SARAH approach (**NORA**-**S**WA**N**-**R**EEF3D-**A**LE-**H**DC) introduces an advanced down-scaling procedure for hydrodynamic analysis, effectively bridging the gap between large-scale offshore metocean data and site-specific coastal engineering applications over varying bathymetric conditions. By integrating multiple numerical wave models at different scales, each with varying levels of physical complexity, the approach ensures minimal information loss while delivering detailed insights into wave transformation and wave loads under relevant hydrodynamic events. This multi-scale modeling strategy strikes a balance between computational efficiency and accuracy, making it a practical and robust tool for coastal engineering applications.

The framework leverages the open-access hindcast database NORA3, the open-source phase-averaging model SWAN, and the open-source hydrodynamic model REEF3D. Within this structure, REEF3D's comprehensive coastal wave suite enables high-resolution wave transformations through a fully nonlinear potential flow model, facilitates extreme event screening via ALE force estimation, and provides high-fidelity CFD simulations to resolve complex wave-breaking and flow interactions. The seamless integration of non-viscous and viscous solvers over irregular bathymetry showcases a strong hydrodynamic coupling (HDC) capability, further enhancing the model's applicability in real-world scenarios.

A case study in southern Norway demonstrates the effectiveness of the NORA-SARAH approach, analyzing slamming wave loads on a navigation tower and wave diffraction at an anchorage. The findings highlight key aspects of wave modeling, including the tendency of phase-averaged methods to underpredict wave diffraction compared to phase-resolving approaches. Moreover, the study reinforces the notion that wave height alone is not a sufficient predictor of wave loads—wave kinematics play a crucial role, particularly in breaking wave impacts. The integration of ALE extreme event identification (EEI) with HDC analysis emphasizes the necessity of the complete down-scaling process, while also showcasing significant time efficiency gains, as only a limited domain and time window require CFD-level analysis. Furthermore, the framework's open accessibility provides a valuable blueprint for adaptation, fostering future developments toward automation. When fully automated, the NORA-SARAH framework holds the potential to become an integral component of data-driven design optimization and serve as a foundation for digital twin applications.

Compared to traditional H_s and spectrum-based design methodologies, the NORA-SARAH approach offers several distinct advantages:

- Better-resolved diffraction;
- Fast extreme wave load identification;
- Detailed breaking wave structures and near-field hydrodynamics
- Balance between computational efficiency and the level of details and accuracy
- An open and streamlined framework for easy adaptation and automation

In the present study, the input waves for both phase-averaging and phase-resolving models are parametrized using H_s and T_p from the

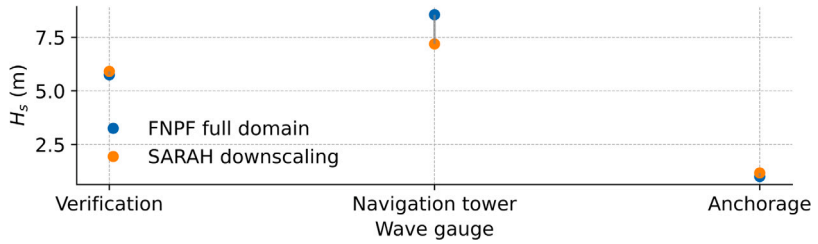

Fig. 13. The differences between the full phase-resolving solution and the down-scale approach.

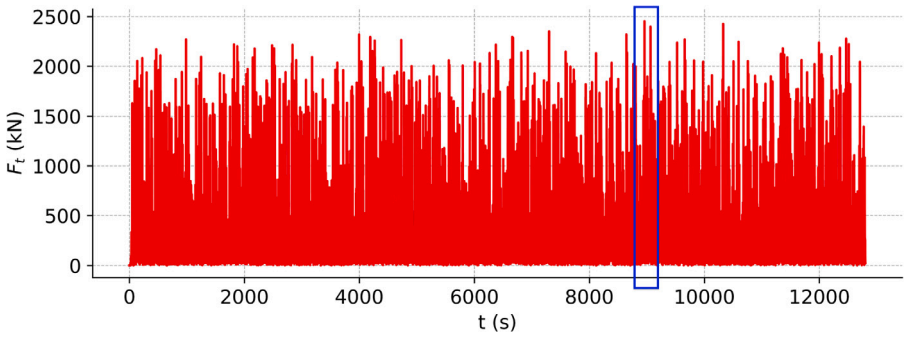

Fig. 14. Total forces on the navigation tower estimated with the NORA-SARAH method in the REEF3D::FNPF NWT.

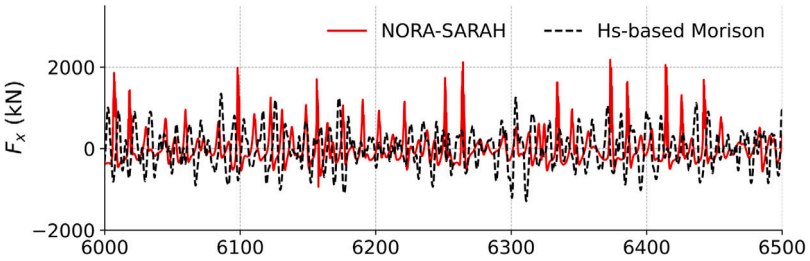

Fig. 15. The x-direction inline force comparison between the presented NORA-SARAH approach and the traditional H_s-based Marison force calcualtion.

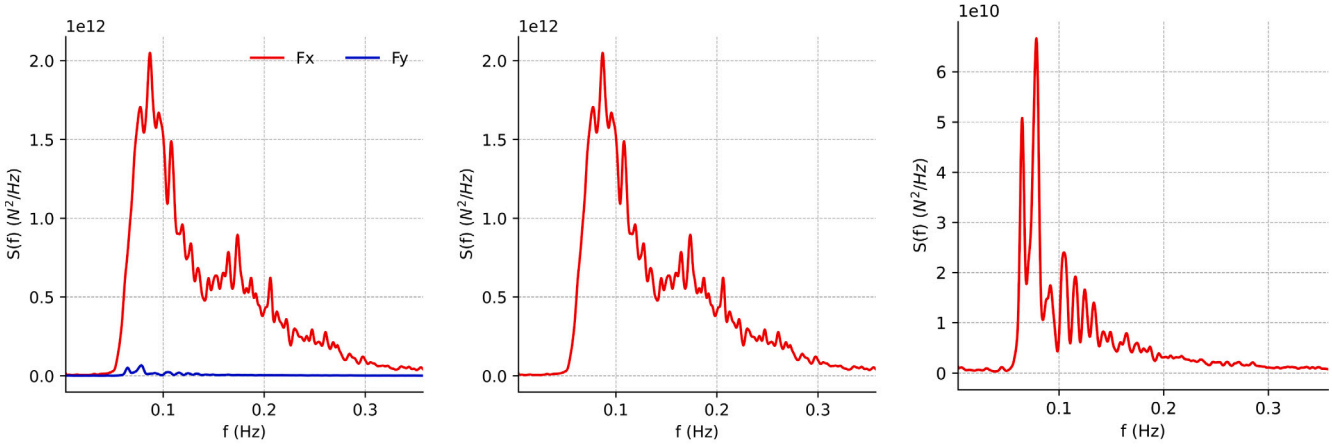

(a) Force spectra in both directions (b) Force spectra in the x-direction (c) Force spectra in the y-direction

Fig. 16. Wave force spectra in the x and y directions at Lyngholmsboen.

upper-level scale, besides the HDC within REEF3D. However, ongoing developments aim to enhance the framework by directly transferring both frequency and directional spectra across the down-scaling process and among numerical models. Additionally, future enhancements include modular batch boundary conditions for multi-stressor, multi-system simulations. These improvements will enable the analysis of interacting wave systems from different principal directions and incorporate the effects of currents and wind on wave fields, further strengthening the applicability and accuracy of the proposed methodology. In many coastal regions, local wind forcing plays a significant role in shaping the wave field. The phase-averaged model SWAN can efficiently account for wind effects, whereas incorporating wind forcing

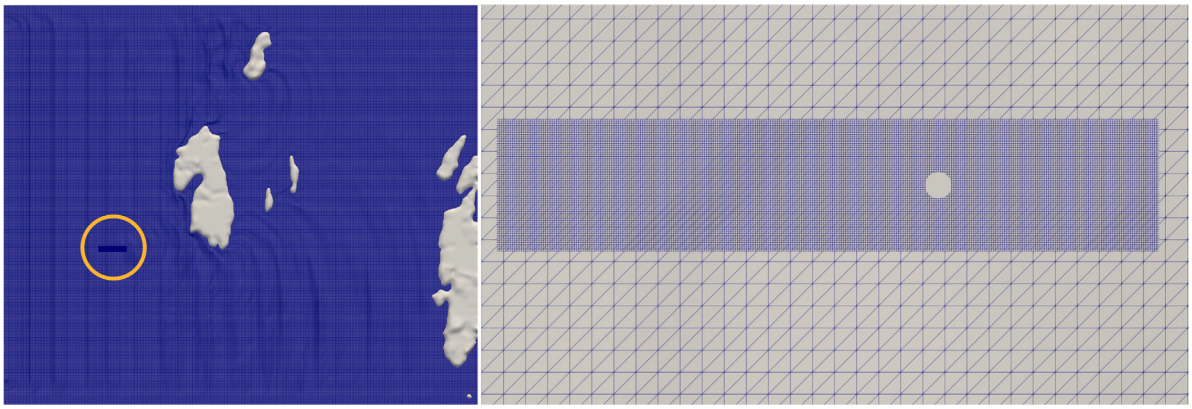

Fig. 17. The mesh configurations in the potential flow and CFD domain, left: the horizontal mesh in the entire phase-resolving domain, where the CFD domain is highlighted by an oragen circle; right: the CFD mesh near the cylinder.

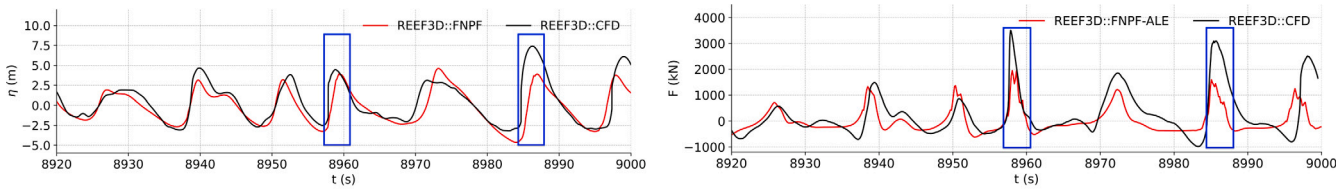

(a) free surface elevation comparison (b) Wave force comparison

Fig. 18. Comparison of the free surface elevation and total wave force at the navigation tower between FNPF and HDC&CFD simulations.

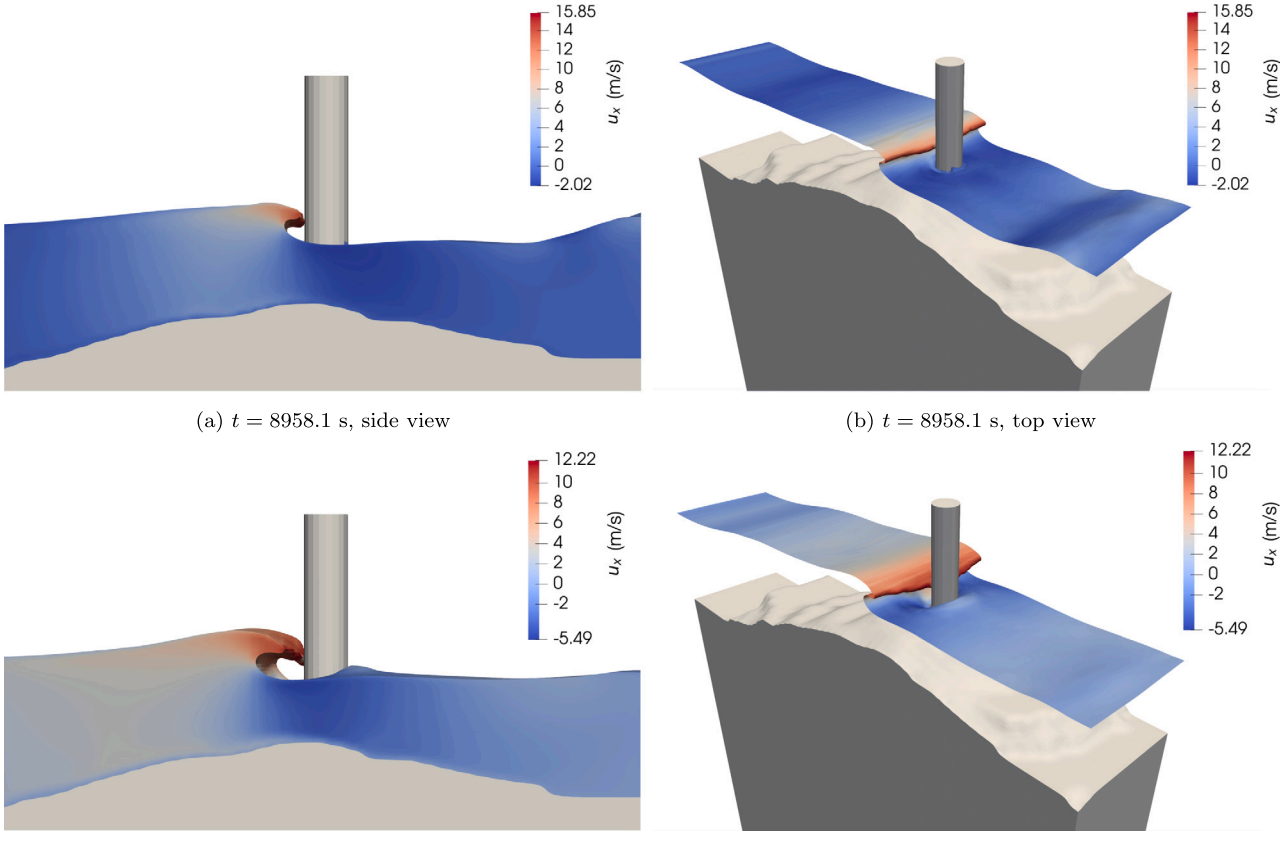

(a) $t = 8958.1$ s, side view (b) $t = 8958.1$ s, top view

(c) $t = 8985.0$ s, side view (d) $t = 8985.0$ s, top view

Fig. 19. The surface elevation rendered with the particle velocity magnitude at the two extreme wave load events at $t = 8958.1$ s and $t = 8985.0$ s in the CFD simulation through the HDC protocol.

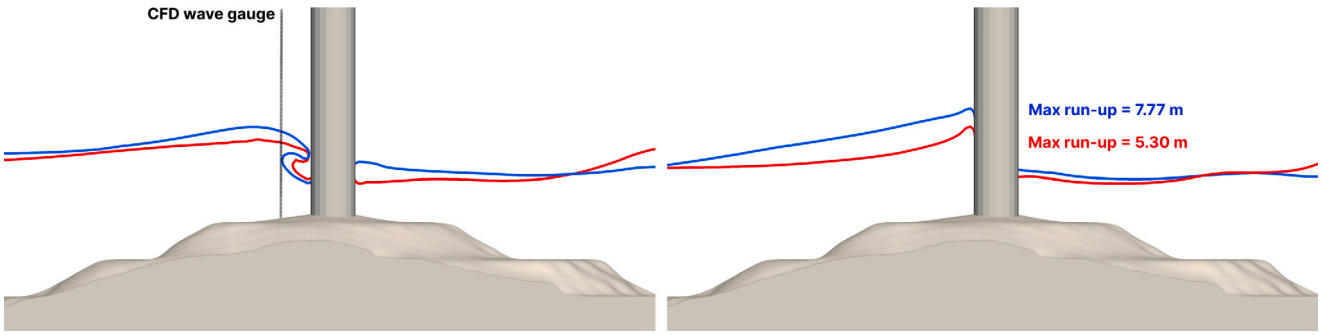

(a) moment of breaking wave impact (b) moment of maximum runup

Fig. 20. Comparison for the free surface elevation profiles simulated with REEF3D::CFD for the moment of breaking wave impacts and the moment of maximum runup at the two extreme events. The red lines represent the first extreme event at $t = 8958.1$ s and the blue lines represent the second extreme event at $t = 8985.0$ s.

in phase-resolving potential flow models remains challenging. In such cases, SWAN plays a key role in representing wind-wave energy transfer, and the downscaling strategy relies on the complementary strengths of the two numerical models.

The NORA-SARAH approach represents a significant step forward in high-fidelity coastal engineering modeling. Its ability to integrate multi-scale hydrodynamic processes while maintaining computational efficiency makes it a valuable tool for engineers and researchers alike. With continued development, this open framework has the potential to revolutionize the way wave-induced hydrodynamic forces are analyzed and optimized in coastal and offshore environments. The recent GPU-accelerated hypre solver (Sahasrabudhe et al., 2021) can further enhance the computational efficiency in solving the Laplace equation in the FNPF solver and Poisson equation in the CFD solver, thus accelerate the entire process. Moreover, this approach exhibits strong synergy with data generation processes and can support machine-learning-based phase-resolved wave prediction, as attempted by Wang et al. (2025). As DNORA also includes functions to downscale global reanalysis datasets such as ERA5, the proposed approach can be straightforwardly extended to applications in most regions of the world.

CRediT authorship contribution statement

Widar Weizhi Wang: Writing – original draft, Visualization, Methodology, Investigation, Formal analysis, Conceptualization. **Konstantinos Christakos:** Writing – review & editing, Conceptualization. **Csaba Pákozdi:** Methodology. **Hans Bihs:** Writing – review & editing, Software, Resources, Project administration, Funding acquisition.

Declaration of competing interest

The authors declare that they have no known competing financial interests or personal relationships that could have appeared to influence the work reported in this paper.

Acknowledgments

The simulations were performed on the supercomputer Betzy provided by UNINETT Sigma2 - the National Infrastructure for High-Performance Computing and Data Storage in Norway. The authors also thank the funding by the European Union (ERC, PARTRES, 101045646). Views and opinions expressed are however those of the authors only and do not necessarily reflect those of the European Union or the European Research Council Executive Agency. Neither the European Union nor the granting authority can be held responsible for them.

Data availability

Data will be made available on request.

References

Aarnes, O.J., Breivik, Ø., Reistad, M., 2012. Wave extremes in the northeast Atlantic. J. Clim. 25 (5), 1529–1543. http://dx.doi.org/10.1175/JCLI-D-11-00132.1.

Aggarwal, A., Alagan Chella, M., Bihs, H., Myrhaug, D., 2020. Properties of breaking irregular waves over slopes. Ocean Eng. (ISSN: 0029-8018) 216, 108098. http://dx.doi.org/10.1016/j.oceaneng.2020.108098.

Aggarwal, A., Bihs, H., Shirinov, S., Myrhaug, D., 2019. Estimation of breaking wave properties and their interaction with a jacket structure. J. Fluids Struct. 91, 102722.

Alagan Chella, M., Bihs, H., D., M., 2019. Numerical modeling of breaking wave kinematics and wave impact pressures on a vertical slender cylinder. J. Fluids Struct. 86, 94–123.

Ashby, S.F., Flagout, R.D., 1996. A parallel mulitgrid preconditioned conjugate gradient algorithm for groundwater flow simulations. Nucl. Sci. Eng. 124 (1), 145–159.

Baquet, A., Kim, J., Huang, Z.J., 2017a. Numerical modeling using CFD and potential wave theory for three-hour nonlinear irregular wave simulations. In: 36th International Conference on Ocean, Offshore and Arctic Engineering, OMAE, Trondheim, Norway.

Baquet, A., Kim, J., Huang, Z., 2017b. Numerical modeling using CFD and potential wave theory for three-hour nonlinear irregular wave simulations. In: International Conference on Offshore Mechanics and Arctic Engineering. Volume 1: Offshore Technology, V001T01A002. http://dx.doi.org/10.1115/OMAE2017-61090.

Bihs, H., Kamath, A., Alagan Chella, M., Aggarwal, A., Arntsen, Ø.A., 2016. A new level set numerical wave tank with improved density interpolation for complex wave hydrodynamics. Comput. & Fluids 140, 191–208. http://dx.doi.org/10.1016/j.compfluid.2016.09.012.

Bihs, H., Wang, W., Pákozdi, C., Kamath, A., 2020. REEF3D::FNPF—A flexible fully nonlinear potential flow solver. J. Offshore Mech. Arct. Eng. (ISSN: 0892-7219) 142 (4), 041902. http://dx.doi.org/10.1115/1.4045915.

Bingham, H.B., Zhang, H., 2007. On the accuracy of finite-difference solutions for nonlinear water waves. J. Engrg. Math. (ISSN: 00220833) 58 (1), 211–228. http://dx.doi.org/10.1007/s10665-006-9108-4.

Bonnefoy, F., Le Touzé, D., Ferrant, P., 2006a. A fully-spectral 3D time-domain model for second-order simulation of wavetank experiments. Part a: Formulation, implementation and numerical properties. Appl. Ocean Res. (ISSN: 0141-1187) 28 (1), 33–43. http://dx.doi.org/10.1016/j.apor.2006.05.004.

Bonnefoy, F., Le Touzé, D., Ferrant, P., 2006b. A fully-spectral 3D time-domain model for second-order simulation of wavetank experiments. Part B: Validation, calibration versus experiments and sample applications. Appl. Ocean Res. (ISSN: 0141-1187) 28 (2), 121–132. http://dx.doi.org/10.1016/j.apor.2006.05.003.

Booij, N., Ris, R.C., Holthuijsen, L.H., 1999. A third-generation wave model for coastal regions: 1. Model description and validation. J. Geophys. Res.: Ocean. 104 (C4), 7649–7666. http://dx.doi.org/10.1029/98JC02622.

Breivik, Ø., Carrasco, A., Haakenstad, H., Aarnes, O.J., Behrens, A., Bidlot, J.-R., Björkqvist, J.-V., Bohlinger, P., Furevik, B.R., Staneva, J., Reistad, M., 2022. The impact of a reduced high-wind charnock parameter on wave growth with application to the North Sea, the Norwegian Sea, and the Arctic Ocean. J. Geophys. Res.: Ocean. 127 (3), e2021JC018196. http://dx.doi.org/10.1029/2021JC018196.

Cheng, Z., Svangstu, E., Moan, T., Gao, Z., 2021. Assessment of inhomogeneity in environmental conditions in a Norwegian fjord for design of floating bridges. Ocean Eng. (ISSN: 0029-8018) 220, 108474. http://dx.doi.org/10.1016/j.oceaneng.2020.108474.

Chorin, A., 1968. Numerical solution of the Navier–Stokes equations. Math. Comp. 22, 745–762.
Christakos, K., Björkqvist, J.-V., Byermoen, E., Furevik, B., 2023. DNORA: an open-source tool for high resolution dynamical downscaling of ocean waves. A storm case in sulafjorden. http://dx.doi.org/10.13140/RG.2.2.34638.95044.
Christakos, K., Gao, Z., Furevik, B.R., Björkqvist, J.-V., Aarnes, O.J., 2022. In situ coastal observations of wave homogeneity and coherence. Appl. Ocean Res. (ISSN: 0141-1187) 129, 103390. http://dx.doi.org/10.1016/j.apor.2022.103390.
Dempwolff, L.-C., Windt, C., Bihs, H., Melling, G., Holzwarth, I., Goseberg, N., 2023. Hydrodynamic coupling of multi-fidelity solvers in REEF3D with application to ship-induced wave modelling. Coast. Eng. (ISSN: 0378-3839) 104452. http://dx.doi.org/10.1016/j.coastaleng.2023.104452.
Donea, J., Huerta, A., Ponthot, J.-P., Rodriguez-Ferran, A., 2004. Arbitrary Lagrangian–Eulerian methods. In: The Encyclopedia of Computational Mechanics. Vol. 1, Wiley, pp. pp. 413–437. http://dx.doi.org/10.1002/0470091355.ecm009, (Chapter 14).
Ducrozet, G., Bonnefoy, F.é.l., Le Touzé, D., Ferrant, P., 2012. A modified high-order spectral method for wavemaker modeling in a numerical wave tank. Eur. J. Mech. B Fluids 34, 19–34. http://dx.doi.org/10.1016/j.euromechflu.2012.01.017.
Ducrozet, G., Bonnefoy, F., Le Touzé, D., Ferrant, P., 2016. HOS-ocean: Open-source solver for nonlinear waves in open ocean based on high-order spectral method. Comput. Phys. Comm. 203, 245–254. http://dx.doi.org/10.1016/j.cpc.2016.02.017.
Engsig-Karup, A., Bingham, H., Lindberg, O., 2009. An efficient flexible-order model for 3D nonlinear water waves. J. Comput. Phys. 228, 2100–2118.
Engsig-Karup, A.P., Madsen, M.G., Glimberg, S.L., 2012. A massively parallel GPU-accelerated model for analysis of fully nonlinear free surface waves. Internat. J. Numer. Methods Fluids 70 (1).
Furevik, B.R., Haakenstad, H., 2012. Near-surface marine wind profiles from rawinsonde and NORA10 hindcast. J. Geophys. Res.: Atmospheres 117 (D23), http://dx.doi.org/10.1029/2012JD018523.
Gobbi, M.F., Kirby, J.T., Wei, G., 2000. A fully nonlinear Boussinesq model for surface waves. Part 2. Extension to O(kh)4. J. Fluid Mech. 405, 181–210. http://dx.doi.org/10.1017/S0022112099007247.
Grilli, S.T., Guyenne, P., Dias, F., 2001. A fully non-linear model for three-dimensional overturning waves over an arbitrary bottom. Internat. J. Numer. Methods Fluids 35 (7), 829–867. http://dx.doi.org/10.1002/1097-0363(20010415)35:7<829::AID-FLD115>3.0.CO;2-2.
Grilli, S.T., Subramanya, R., Svendsen, I.A., Veeramony, J., 1994. Shoaling of solitary waves on plane beaches. J. Waterw. Port Coast. Ocean. Eng. 120 (6), 609–628.
Haakenstad, H., Breivik, Ø., Furevik, B.R., Reistad, M., Bohlinger, P., Aarnes, O.J., 2021. NORA3: A nonhydrostatic high-resolution hindcast of the North Sea, the Norwegian Sea, and the Barents Sea. J. Appl. Meteorol. Clim. 60 (10), 1443–1464. http://dx.doi.org/10.1175/JAMC-D-21-0029.1.
Haakenstad, H., Breivik, Ø., Reistad, M., Aarnes, O.J., 2020. NORA10EI: a revised regional atmosphere-wave hindcast for the North Sea, the Norwegian Sea and the Barents Sea. Int. J. Climatol. 40 (10), 4347–4373. http://dx.doi.org/10.1002/joc.6458.
Hasselmann, K., Barnett, T., Bouws, E., Carlson, H., Cartwright, D., Enke, K., Ewing, J., Gienapp, H., Hasselmann, D., Kruseman, P., Meerburg, A., Müller, P., Olbers, D., Richter, K., Sell, W., Walden, H., 1973. Measurements of wind-wave growth and swell decay during the joint north sea wave project (JONSWAP). Ergänzungsheft Dtsch. Hydrogr. Z. Reihe A 12 (8), 1–95.
Holthuijsen, L., Herman, A., Booij, N., 2003. Phase-decoupled refraction–diffraction for spectral wave models. Coast. Eng. (ISSN: 0378-3839) 49 (4), 291–305. http://dx.doi.org/10.1016/S0378-3839(03)00065-6.
Hughes, S.A., 1984. The TMA Shallow-Water Spectrum Description and Applications. Tech. Rep. CERC-84-7, Coastal Engineering Research Center, Vicksburg, Mississippi, U.S.A..
Jacobsen, N.G., Fuhrman, D.R., Fredsœ, J., 2012. A wave generation toolbox for the open-source CFD library: OpenFOAM. Internat. J. Numer. Methods Fluids 70 (9), 1073–1088.
Jeschke, A., Pedersen, G.K., Vater, S., Behrens, J., 2017. Depth-averaged non-hydrostatic extension for shallow water equations with quadratic vertical pressure profile: equivalence to Boussinesq-type equations. Internat. J. Numer. Methods Fluids 84 (10), 569–583. http://dx.doi.org/10.1002/fld.4361.
Jiang, G.S., Shu, C.W., 1996. Efficient implementation of weighted ENO schemes. J. Comput. Phys. 126, 202–228.
Kamath, A., Wang, W., Pakozdi, C., Bihs, H., 2023. Identification and Investigation of Extreme Events Using an Arbitrary Lagrangian–Eulerian Approach With a Laplace Equation Solver and Coupling to a Navier–Stokes Solver. J. Offshore Mech. Arct. Eng. (ISSN: 0892-7219) 145 (6), 061902. http://dx.doi.org/10.1115/1.4057014.
Laflèche, S., Christakos, K., Ommani, B., Fouques, S., Kristiansen, T., 2024. Experimental reproduction of inhomogeneous fjord waves. Coast. Eng. (ISSN: 0378-3839) 189, 104492. http://dx.doi.org/10.1016/j.coastaleng.2024.104492.
Larsen, J., Dancy, H., 1983. Open boundaries in short wave simulations - a new approach. Coast. Eng. 7, 285–297.
Li, B., Fleming, C.A., 1997. A three dimensional multigrid model for fully nonlinear water waves. Coast. Eng. (ISSN: 0378-3839) 30 (3), 235–258. http://dx.doi.org/10.1016/S0378-3839(96)00046-4.
Lynett, P., Liu, P.L.-F., 2004. A two-layer approach to wave modelling. Proc. R. Soc. Lond. Ser. A Math. Phys. Eng. Sci. 460 (2049), 2637–2669. http://dx.doi.org/10.1098/rspa.2004.1305.
Madsen, P.A., Bingham, H.B., Liu, H., 2002. A new Boussinesq method for fully nonlinear waves from shallow to deep water. J. Fluid Mech. 462, 1–30.
Madsen, P.A., Murray, R., Sørensen, O.R., 1991. A new form of the Boussinesq equations with improved linear dispersion characteristics. Coast. Eng. 15, 371–388.
Madsen, P.A., Schäffer, H.A., 1998. Higher-order Boussinesq-type equations for surface gravity waves: derivation and analysis. Philos. Trans. R. Soc. Lond. Ser. A Math. Phys. Eng. Sci. 356 (1749), 3123–3181. http://dx.doi.org/10.1098/rsta.1998.0309.
Madsen, P.A., Sørensen, O.R., 1992. A new form of the Boussinesq equations with improved linear dispersion characteristics. Part 2. A slowly-varying bathymetry. Coast. Eng. (ISSN: 0378-3839) 18 (3), 183–204. http://dx.doi.org/10.1016/0378-3839(92)90019-Q.
Mayer, S., Garapon, A., Sørensen, L.S., 1998. A fractional step method for unsteady free surface flow with applications to non-linear wave dynamics. Internat. J. Numer. Methods Fluids (ISSN: 1097-0363) 28 (2), 293–315. http://dx.doi.org/10.1002/(SICI)1097-0363(19980815)28:2<293::AID-FLD719>3.0.CO;2-1.
Monteban, D., 2016. Numerical Modelling of Wave Agitation in Ports and Access Channels (Master's thesis). Delft University of Technology.
Morison, J.R., Johnson, J.W., O'Brien, M.P., 1954. Experimental studies of wave forces on piles. In: Proc., 4th Coastal Engineering Conference.
Nwogu, O., 1993. Alternative form of Boussinesq equations for nearshore wave propagation. J. Waterw. Port Coast. Ocean. Eng. 119 (6), 618–638.
Osher, S., Sethian, J.A., 1988. Fronts propagating with curvature- dependent speed: algorithms based on Hamilton–Jacobi formulations. J. Comput. Phys. 79, 12–49.
Pákozdi, C., Kamath, A., Wang, W., Bihs, H., 2022. Application of arbitrary Lagrangian–Eulerian strips with fully nonlinear wave kinematics for force estimation. Mar. Struct. (ISSN: 0951-8339) 83, 103190. http://dx.doi.org/10.1016/j.marstruc.2022.103190.
Pakozdi, C., Kamath, A., Wang, W., Martin, T., Bihs, H., 2022. Efficient calculation of hydrodynamic loads on offshore wind substructures including slamming forces. J. Offshore Mech. Arct. Eng. (ISSN: 0892-7219) 145 (2), 021901. http://dx.doi.org/10.1115/1.4055701.
Paulsen, B.T., Bredmose, H., Bingham, H.B., 2014. An efficient domain decomposition strategy for wave loads on surface piercing circular cylinders. Coast. Eng. 86, 57–76.
Pierson, W.J., Moskowitz, L., 1964. A proposed spectral form for fully developed wind seas based on the similarity theory of S. A. Kitaigorodskii. J. Geophys. Res. (ISSN: 2156-2202) 69 (24), 5181–5190. http://dx.doi.org/10.1029/JZ069i024p05181.
Raoult, C., Benoit, M., Yates, M.L., 2016. Validation of a fully nonlinear and dispersive wave model with laboratory non-breaking experiments. Coast. Eng. (ISSN: 0378-3839) 114, 194–207. http://dx.doi.org/10.1016/j.coastaleng.2016.04.003.
Reistad, M., Breivik, Ø., Haakenstad, H., Aarnes, O.J., Furevik, B.R., Bidlot, J.-R., 2011. A high-resolution hindcast of wind and waves for the North Sea, the Norwegian Sea, and the Barents Sea. J. Geophys. Res.: Ocean. 116 (C5), http://dx.doi.org/10.1029/2010JC006402.
Sahasrabudhe, D., Zambre, R., Chandramowlishwaran, A., Berzins, M., 2021. Optimizing the hypre solver for manycore and GPU architectures. J. Comput. Sci. (ISSN: 1877-7503) 49, 101279. http://dx.doi.org/10.1016/j.jocs.2020.101279.
Shu, C.W., Osher, S., 1988. Efficient implementation of essentially non-oscillatory shock capturing schemes. J. Comput. Phys. 77, 439–471.
Simon, B., Papoutsellis, C.E., Benoit, M., Yates, M.L., 2019. Comparing methods of modeling depth-induced breaking of irregular waves with a fully nonlinear potential flow approach. J. Ocean. Eng. Mar. Energy (ISSN: 2198-6452) http://dx.doi.org/10.1007/s40722-019-00154-7.
Smit, P., Zijlema, M., Stelling, G., 2013. Depth-induced wave breaking in a non-hydrostatic, near-shore wave model. Coast. Eng. (ISSN: 0378-3839) 76, 1–16. http://dx.doi.org/10.1016/j.coastaleng.2013.01.008.
Stelling, G.S., Duinmeijer, S.P.A., 2003. A staggered conservative scheme for every Froude number in rapidly varied shallow water flows. Internat. J. Numer. Methods Fluids 43 (12), 1329–1354. http://dx.doi.org/10.1002/fld.537.
Tolman, H.L., Chalikov, D., 1996. Source terms in a third-generation wind wave model. J. Phys. Oceanogr. 26 (11), 2497–2518.
van der Vorst, H., 1992. BiCGStab: A fast and smoothly converging variant of bi-CG for the solution of nonsymmetric linear systems. SIAM J. Sci. Stat. Comput. 13, 631–644.
Wang, W., 2020. Large-Scale Phase-Resolved Wave Modelling for the Norwegian Coast (Ph.D. thesis). Norwegian University of Science and Technology, Trondheim, Norway, URL https://ntnuopen.ntnu.no/ntnu-xmlui/handle/11250/2673803.
Wang, W.W., Christakos, K., Bihs, H., 2025. AI-Powered Down-Scale Wave Hydrodynamic Analysis for Coastal Marine Structures. In: International Conference on Offshore Mechanics and Arctic Engineering, Volume 3: Ocean Engineering; Polar and Arctic Sciences and Technology, V003T06A077. http://dx.doi.org/10.1115/OMAE2025-156465.
Wang, W., Kamath, A., Martin, T., Pákozdi, C., Bihs, H., 2020a. A comparison of different wave modelling techniques in an open-source hydrodynamic framework. J. Mar. Sci. Eng. (ISSN: 2077-1312) 8, 7. http://dx.doi.org/10.3390/jmse8070526.
Wang, W., Kamath, A., Pakozdi, C., Bihs, H., 2019. Investigation of focusing wave properties in a numerical wave tank with a fully nonlinear potential flow model. J. Mar. Sci. Eng. (ISSN: 2077-1312) 7 (10), http://dx.doi.org/10.3390/jmse7100375.
Wang, W., Martin, T., Kamath, A., Bihs, H., 2020b. An improved depth-averaged non-hydrostatic shallow water model with quadratic pressure approximation. Internat. J. Numer. Methods Fluids 92, 803–824. http://dx.doi.org/10.1002/fld.4807.

Wang, W., Pákozdi, C., Kamath, A., Bihs, H., 2021a. A fully nonlinear potential flow wave modelling procedure for simulations of offshore sea states with various wave breaking scenarios. Appl. Ocean Res. (ISSN: 0141-1187) 117, 102898. http://dx.doi.org/10.1016/j.apor.2021.102898.

Wang, W., Pákozdi, C., Kamath, A., Bihs, H., 2021b. Representation of 3-h offshore short-crested wave field in the fully nonlinear potential flow model REEF3D::FNPF. J. Offshore Mech. Arct. Eng. (ISSN: 0892-7219) 144 (4), 041902. http://dx.doi.org/10.1115/1.4053774.

Wang, W., Pákozdi, C., Kamath, A., Fouques, S., Bihs, H., 2022a. A flexible fully nonlinear potential flow model for wave propagation over the complex topography of the norwegian coast. Appl. Ocean Res. (ISSN: 0141-1187) 122, 103103. http://dx.doi.org/10.1016/j.apor.2022.103103.

Wang, W., Pákozdi, C., Kamath, A., Martin, T., Bihs, H., 2021c. Hydrodynamic Coupling of Viscous and Non-Viscous Numerical Wave Solutions Within the Open-Source Hydrodynamics Framework REEF3D. In: International Conference on Offshore Mechanics and Arctic Engineering, Volume 8: CFD and FSI, http://dx.doi.org/10.1115/OMAE2021-62185.

Wang, W., Pákozdi, C., Kamath, A., Martin, T., Bihs, H., 2022b. Hydrodynamic coupling of viscous and non-viscous numerical wave solutions within the open-source hydrodynamics framework REEF3D. J. Offshore Mech. Arct. Eng. (ISSN: 0892-7219) 144 (4), http://dx.doi.org/10.1115/1.4053848, 041903.

Wei, G., Kirby, J.T., Grilli, S.T., Subramanya, R., 1995. A fully nonlinear Boussinesq model for surface waves. Part 1. Highly nonlinear unsteady waves. J. Fluid Mech. 294, 71–92. http://dx.doi.org/10.1017/S0022112095002813.

Wilcox, D.C., 1994. Turbulence Modeling for CFD. DCW Industries Inc., La Canada, California.

Yates, M.L., Benoit, M., 2015. Accuracy and efficiency of two numerical methods of solving the potential flow problem for highly nonlinear and dispersive water waves. Internat. J. Numer. Methods Fluids 77 (10), 616–640. http://dx.doi.org/10.1002/fld.3992.

Zhang, J., Benoit, M., Kimmoun, O., Chabchoub, A., Hsu, H.-C., 2019. Statistics of extreme waves in coastal waters: Large scale experiments and advanced numerical simulations. Fluids (ISSN: 2311-5521) 4 (2), http://dx.doi.org/10.3390/fluids4020099.

Zijlema, M., Stelling, G.S., 2005. Further experiences with computing non-hydrostatic free-surface flows involving water waves. Internat. J. Numer. Methods Fluids 48 (2), 169–197. http://dx.doi.org/10.1002/fld.821.

Zijlema, M., Stelling, G., 2008. Efficient computation of surf zone waves using the nonlinear shallow water equations with non-hydrostatic pressure. Coast. Eng. (ISSN: 0378-3839) 55 (780–790), 780–790. http://dx.doi.org/10.1016/j.coastaleng.2008.02.020.

Zijlema, M., Stelling, G., Smit, P., 2011. SWASH: An operational public domain code for simulating wave fields and rapidly varied flows in coastal waters. Coast. Eng. (ISSN: 0378-3839) 58 (10), 992–1012. http://dx.doi.org/10.1016/j.coastaleng.2011.05.015.